

QANet - Quality Assurance Network for Image Segmentation

Assaf Arbelle, Eliav Elul and Tammy Riklin Raviv
The Department of Electrical and Computer Engineering
The Zlotowski Center for Neuroscience
Ben-Gurion University of the Negev

Abstract—Tools and methods for automatic image segmentation are rapidly developing, each with its own strengths and weaknesses. While these methods are designed to be as general as possible, there are no guarantees for their performance on new data. The choice between methods is usually based on benchmark performance whereas the data in the benchmark can be significantly different than that of the user.

We introduce a novel Deep Learning method which, given an image and a corresponding segmentation, obtained by any method including manual annotation, estimates the Intersection over Union measure (IoU) with respect to the *unknown* ground truth. We refer to this method as a Quality Assurance Network - QANet. The QANet is designed to give the user an estimate of the segmentation quality on the users own, private, data without the need for human inspection or labeling. It is based on the RibCage Network architecture, originally proposed as a discriminator in an adversarial network framework. The QANet was trained on simulated data with synthesized segmentations and was tested on real cell images and segmentations obtained by three different automatic methods as submitted to the Cell Segmentation Benchmark. We show that the QANet's predictions of the IoU scores accurately estimates to the IoU scores evaluated by the benchmark organizers based on the ground truth segmentation.

The code is freely available at: TBD.

Index Terms—Deep Learning, Microscopy, Segmentation, Quality Assurance

I. INTRODUCTION

Image segmentation is a well-studied problem, playing a major role in almost any image analysis task. Model-based as well as data-driven approaches are usually validated on ‘previously unseen’ annotated test sets, being compared to benchmarks and current state-of-the-art segmentation methods adapted to the task examined, the imaging modality and depicted scene or objects. Some recent methods manage to achieve almost ‘human-level’ scores on well known challenges and benchmarks. Nevertheless, a measurable and objective evaluation of image segmentation with respect to user specific data is yet to be addressed.

Consider for example live cell microscopy image segmentation. Instance segmentation of individual cells allows the extraction of useful information at the cellular level. Further analysis of this output may shed light on biological processes and phenomena - potentially making a significant impact on health care research. The implications of some of these biological findings are critical, thus every step in the research process, in particular cell segmentation, must be reliable. Online benchmarks, such as the Cell Segmentation Benchmark [16],

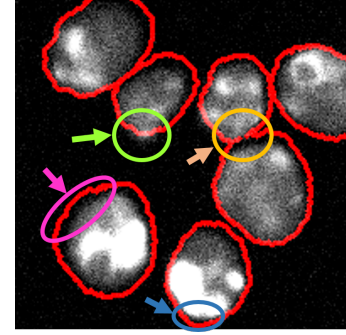


Figure 1. Simulated Training Data: An example of an image with the contours of some segmentation method (red). The errors of the segmentation are encircled with an orange dashed line including errors such as merged cells, dilated segmentation and missed areas.

evaluate, compare and objectively rank multiple automatic methods. Still, the question arises whether one can be assured that a given segmentation method will consistently perform well enough on private data. Moreover, current methods are ranked based on the statistics of the measured score on some specific data set, how could a user detect specific cases of segmentation failures which may risk the overall biological analysis? In other words, can we avoid visual inspection of the results or an additional test with data-specific manual annotations, in this, and alike, important pipelines?

This paper is the first to address (to the best of our knowledge) quantitative assessment of image segmentation *without* ground truth annotations given only the image and its corresponding segmentation. Specifically, we propose a deep neural network, termed Quality Assurance Network - QANet, that is able to estimate the intersection-over-union (IoU) scores of image-segmentation pairs. It should be stressed that QANet *does not* aim to estimate the ground truth (GT) segmentation and compare it with the segmentation to be evaluated. Instead, it solves a regression problem, providing a scalar between zero and one which can be seen as a quality assessment score of the evaluated segmentation.

A human expert can assess the quality of a given segmentation by comparing it to the raw image alone (Figure 1). We show that this ability can be learned by our QANet. In order to facilitate the comparison capability, the QANet is based on a unique architecture, called the RibCage Network, which was first introduced in [2] as a discriminator in an adversarial

setting. The RibCage is designed as a three channel network - two ‘ribs’ and a ‘spine’. Each rib gets as input either the image or the segmentation, and the spine merges the two channels at each layer allowing a multi-level, spatially sensitive comparison of the inputs. We note that this architecture has an advantage over a simple concatenation of the image and its segmentation, which is limited to low level feature comparison. It also outperforms the Siamese architecture in which each input is processed independently and is therefore restricted to the comparison of high level features.

In this work, we specifically address quantitative evaluation of instance segmentation. As opposed to semantic segmentation, we need to consider the partition of an image into an unknown number of similar, possibly overlapping objects with arbitrary labeling. In order to preserve the separation of neighboring instances, we choose to define the segmentation as a trinary image representing foreground, background and instance boundary.

While the QANet’s architecture and its training regime can be applied to any type of data, we chose to validate it on live cell microscopy images. Specifically, we used fluorescence microscopy data sets from the Cell Segmentation Benchmark¹ [16]. Considering the segmentation of **individual cells**, the QANet’s output is an estimate of the average IoU scores calculated for each connected component comprising the evaluated segmentation, as in the benchmark. We trained the network on simulated data, Flou-N2DH-SIM+, and tested it based on the segmentation results of KTH-SE(1) [8] and CVUT-CZ [15] that were among the top three methods in the benchmark on Fluo-N2DH-GOWT1 and Fluo-N2DL-HeLa test datasets. Very promising results are shown. Specifically, the QANet predicted the average IoU score as calculated by the benchmark organizers with maximum relative error of 1%.

The rest of the paper is organized as follows: Section II discusses some related works and highlights the novelty of the task we aim to address. In Section III we formulate the QA problem and quality measure; present the RibCage architecture as well as the loss; and discuss the simulation of training examples. Experimental results are presented in Section IV. Specifically we present results on simulated as well as real data, testing the RibCage with respect to two alternative architectures and binary vs. binary segmentation representations. We conclude in Section V.

II. RELATION TO PREVIOUS WORK

Some Computer Vision methods, not necessarily for image segmentation, produce confidence scores alongside their output. One could argue that the QANet is yet another confidence score. One such example is the YOLO network [11], [12], [13] for example, designed for object detection, which predicts both a bounding box and its estimated IoU. Nevertheless, there are essential differences between the QANet and the YOLO confidence score. Not only is a bounding-box a very crude estimation of the instance segmentation, but while the YOLO’s scoring can be applied only to its own outputs the QANet works on the output of other methods (possibly even

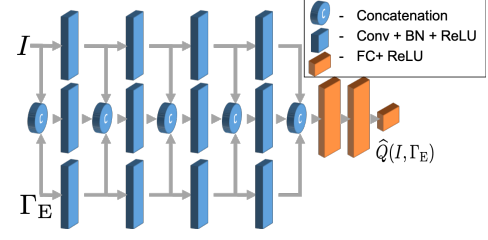


Figure 2. **Network Architecture:** The QANet is designed in the form of a RibCage Network, the top rib processes the raw gray-level image while the bottom rib processes the segmentation proposal. The spine processes the concatenation of the two ribs throughout the depth of the network. The four RibCage blocks are followed by three FC layers which output a single scalar representing the estimated $\hat{Q}_\theta(I, \Gamma_E)$ measure.

the YOLO’s outputs) and scores the output independently of the method creating it.

When considering networks which score the outputs of other networks, the discriminator in an adversarial framework comes to mind [6]. However, we should note that the goal of the discriminator is not to regress the confidence score, but only to preform as an implicit loss function for its adversarial network. It is usually trained for binary classification of "real" versus "fake" examples, and once the training is done, the discriminator collapses and does not produce informative outputs.

III. METHOD

A. Formulation

Our objective is to evaluate multiple instance object segmentation. Let $I: \Omega \rightarrow \mathbb{R}$ be a gray-level image, where Ω is either a 2D or a 3D image domain. Let $\Gamma_{GT}: \Omega \rightarrow \mathbb{L}$ be the corresponding GT segmentation with labels $\mathbb{L} = \{0, 1, 2\}$ corresponding to the background, foreground and object boundaries, respectively. Each connected component of the foreground represents a single instance. We wish to evaluate a proposed segmentation, $\Gamma_E: \Omega \rightarrow \mathbb{L}$, of I . The evaluation criteria can be any segmentation quality measure, i.e., Dice measure [4], IoU [7], Housdorff distance [5], etc. We denote the true quality measure for a pair of GT and proposed segmentation as $Q(\Gamma_{GT}, \Gamma_E)$. Our goal is to estimate the quality measure given only the raw image I and the evaluated segmentation Γ_E denoted as $\hat{Q}(I, \Gamma_E)$.

B. RibCage Network Architecture and Loss

Let $\hat{Q}_\theta(I, \Gamma_E)$ denote the QANet with parameters θ . The QANet is implemented using the RibCage architecture [2]. The strength of this architecture is its ability to extract and compare multilevel features from two inputs in a spatially sensitive manner over multiple scales. The RibCage architecture, outlined in Figure 2, is comprised of blocks of two ribs connected to a spine. The spine merges the two ribs’ outputs. Each of the three channels is passed through a strided convolutional layer, batch normalization and a ReLU activation.

The equations for the l^{th} rib-cage block, where $l \in [1, L]$ and L is number of rib-cage blocks. The inputs r_1^{l-1} , r_2^{l-1} and s^{l-1} represent the two ribs and the spine respectively:

$$r_1^l = f(\theta_{r_1^l} * r_1^{l-1}) \quad (1)$$

¹<http://celltrackingchallenge.net/latest-csb-results/>

$$r_2^l = f(\theta_{r_2^l} * r_2^{l-1}) \quad (2)$$

$$s^l = f(\theta_s * s^{l-1} + \theta_{s1} * r_1^{l-1} + \theta_{s2} * r_2^{l-1}) \quad (3)$$

where the function $f(\cdot)$ represents the Batch Normalization and the ReLU activation. The initial inputs r_1^0, r_2^0 are set to be the image I and the segmentation Γ_E . The spine input is set to be $s^0 = 0$. The outputs of the last block L are then passed to several FC layers resulting in a single scalar \hat{Q}_θ .

The QANet is trained to regress the values of some pre-defined quality measure, Q . The training loss, \mathcal{L} , is the mean squared error (MSE) between the networks output and the true measure:

$$\mathcal{L} = \|\hat{Q}_\theta(I, \Gamma_E) - Q(\Gamma_{GT}, \Gamma_E)\|_2 \quad (4)$$

C. Simulated Segmentations

The input to the QANet, in both training and test phases, is composed of image-segmentation pairs. In the training phase, we synthesize imperfect segmentation proposals by deforming the given GT segmentations such that the true value of the quality measure, Q , can be calculated. We wish that the deformations will be as realistic as possible, as if they were the output of some segmentation algorithm or an unqualified annotator. The deformation process consists of two stages, erosion/dilation (ED) and non-rigid perturbations.

1) *Erosion/Dilation*: The erosion and dilation simulate under/over-estimation of the object region respectively. We note that after the ED stage an instance may be completely removed or merged with neighboring instances. We randomly sample three-state variable, OP , to decide on either of the operations: erosion, dilation or identity. If either erosion or dilation is selected, we sample a positive integer, σ_{ED} , to define the ED kernel size.

2) *Non-Rigid Perturbations*: Inspired by the data augmentation stage of [14], we randomly sample a vector field map, $[v_x, v_y]$, in the size of the input domain Ω and smooth it using a Gaussian kernel, σ_g . The final deformed segmentation Γ_E is obtained by applying the smoothed vector field map to the segmentation resulting from the ED stage.

IV. EXPERIMENTS

A. Evaluation of the QANet

The MSE between the GT quality value, Q , and the predicted quality value \hat{Q}_θ is the most straight forward measure for evaluating the QANet. However, for demonstrating the QANet performances for different Q values we used a scatter plot showing $Q(\Gamma_{GT}, \Gamma_E)$, with respect to the predicted $\hat{Q}_\theta(I, \Gamma_E)$, for the test examples. In addition, we calculated the Hit Rate - which is the normalized number of test examples of which the differences between Q and \hat{Q}_θ are within a specified tolerance. We also used the Area Under the Curve (AUC) of the Hit Rate versus tolerance plot as another quantitative measure of the evaluation of the QANet.

B. The SEG Measure

The SEG measure, introduced in [9] for microscopy cell segmentation evaluation, is an extension of the IoU measure for multiple instances. The measure first finds a one to one matching between the evaluated object labels and the GT labels, where each matched pair is scored using the IoU measure. Let K and K' be the number of individual cells in the GT and evaluated segmentation, Γ_{GT} and Γ_E respectively. Let $c \in \Gamma_{GT}$ and $c' \in \Gamma_E$ define corresponding connected components in the evaluated and GT segmentations, respectively. The SEG measure is defined as the IoU of the GT and the evaluated objects, unless their overlap is lower than 50%. The mean SEG measure over all GT objects is formulated as follows:

$$Q(\Gamma_{GT}, \Gamma_E) = \frac{1}{K} \sum_{c \in \Gamma_{GT}} \sum_{c' \in \Gamma_E} \begin{cases} IoU(c, c') & \alpha(c, c') > 0.5 \\ 0 & \text{otherwise} \end{cases} \quad (5)$$

where, $IoU(c, c') = \frac{|c \cap c'|}{|c \cup c'|}$ and $\alpha(c, c') = \frac{|c \cap c'|}{|c|}$. We note that for every connected component in $c \in \Gamma_{GT}$ there exists at most one connected component $c' \in \Gamma_E$ with overlap grater than 50%. If there is no such object, the cell is considered undetected and its SEG score is set to zero.

C. Training Data

The input to the QANet, in both training and test phases, is composed of image-segmentation pairs. In the training phase we use simulated images such that the corresponding GT segmentations are known. To synthesize imperfect segmentation proposals we deform the GT segmentations such that the true value of the quality measure, Q , can be calculated. The dataset was split into a training and validation set, 70%-30% respectively.

1) *Simulating Images and GT Segmentations*: The training images and GT segmentations were synthesized using the CytoPacq web service² [17]. We tuned the system to produce data similar to the Fluo-N2DH-SIM+ from the Cell Segmentation Benchmark. The CytoPacq synthesizes the images in three steps: 1) 3D digital phantom simulation that generates spatial objects of interest and their structure. This step defines the GT segmentation Γ_{GT} ; 2) Simulation that models image formation in the optical system; 3) Acquisition device simulation that mimics image capturing process when using digital image detectors. We generated 10000 images of size 420×420 pixels, each image containing between 1 to 60 cells. The data was split to training and validation sets: 80% - 20% respectively.

2) *Synthesizing Imperfect Segmentations*: If OP is either erosion or dilation a random integer is sampled from a integer uniform distribution: $\sigma_{ED} \sim U(1, 4)$ which determines the size of the ED kernel. The non-rigid perturbation is defined by a vector field sampled from a uniform distribution $v_x, v_y \sim U(-512, 512)$ followed by a smoothing with a Gaussian kernel of width $\sigma_g = 38$.

²<https://cbia.fi.muni.cz/simulator>

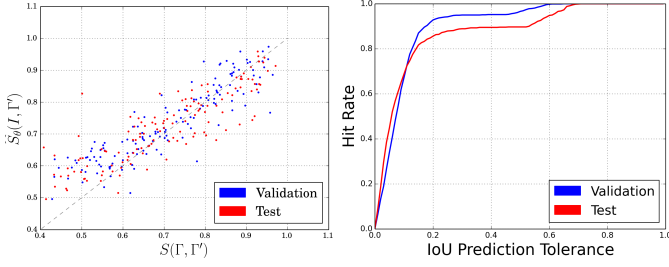


Figure 3. The left image shows the scatter plot of the validation and test images. The horizontal axis is the GT IoU of the instance and the vertical axis show the QANet output. The diagonal line represents the optimal, desired, output. On the right is a Hit Rate curve as a function of IoU prediction tolerance.

D. Test Data

Although the QANet was trained on synthesized images (Section IV-C and simulated segmentations), we tested the method's true capabilities on real data.

1) *Test Images*: In addition to the simulated data detailed in IV-C, we tested our framework with two **real** fluorescent microscopy datasets from the Cell Segmentation Benchmark, namely Fluo-N2DH-GOWT1 and Fluo-N2DL-HeLa. The Fluo-N2DH-GOWT1 dataset is a data of GFP-GOWT1 mouse stem cells acquired by Leica TCS SP5 microscope with pixel size 0.24×0.24 microns [3]. The Fluo-N2DL-HeLa dataset is of HeLa cells stably expressing H2b-GFP acquired by Olympus IX81 microscope with pixel size 0.645×0.645 microns [10].

2) *Test Segmentations*: The test segmentations were generated using three state-of-the-art cell segmentation methods applied to the test images. These include two Deep Learning based methods CVUT-CZ [15] and BGU-IL(3) [1], and a classical method KTH-SE(1) [8]. All methods were downloaded from the Cell Segmentation Benchmark website. In the following experiments we refer to the four method-dataset combinations as: KTH-GOWT1 and KTH-HeLa - result obtained by running the KTH-SE(1) method on Fluo-N2DH-GOWT1 and Fluo-N2DL-HeLa datasets respectively; CVUT-GOWT1 and CVUT-HeLa - result obtained by running the CVUT-CZ method on Fluo-N2DH-GOWT1 and Fluo-N2DL-HeLa datasets respectively.

E. Network Architecture Experiment

We compare three alternative architectures for the QANet, the proposed RibCage, the Siamese and the naive feed forward networks. In our experiments, all the layers have the same number of features and end with three FC layers. The networks differ in the first four layers:

The RibCage network is composed of four rib-cage blocks followed by three FC layers as described as in Section III-B.

The Siamese network is comprised of two independent streams of four convolutional layers, one getting I as input and the other Γ_E . The outputs of the last convolutional layers are concatenated and fed into the FC layers.

The naive network gets a single input, the concatenation on the channel axis of the gray-scale image with evaluated

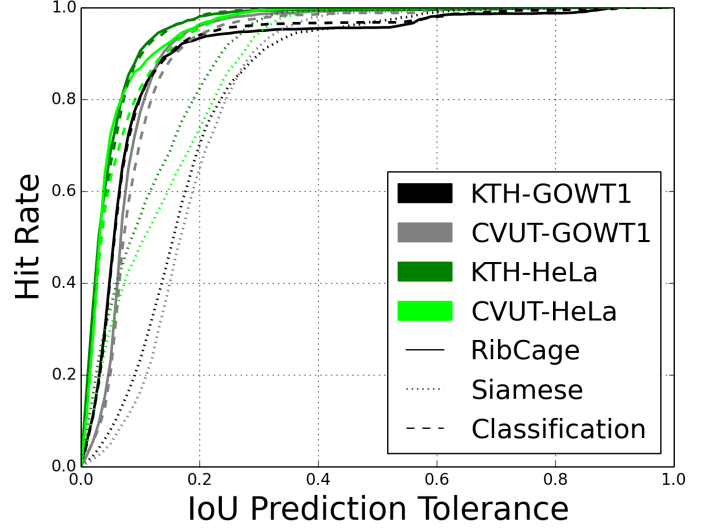


Figure 4. The Hit Rate curves as a function of SEG prediction tolerance. The plot shows the comparison of the three network architectures, namely RibCage (full line), Siamese (dotted line) and Naive (dashed line) networks. All configurations were tested using two segmentation methods: KTH-SE(1) (black and dark green) and CVUT-CZ (gray and light green), on two datasets: Fluo-N2DH-GOWT1 (black and gray) and Fluo-N2DL-HeLa (dark and light green).

segmentation image, I and Γ_E . It is comprised of four convolutional layers followed by the FC layers.

We tested the tree alternatives on the outputs of the CVUT-CZ and the KTH-SE(1) methods applied to two datasets: Fluo-N2DH-GOWT1 and Fluo-N2DL-HeLa as described in Section IV-D. The Hit Rate curves and the corresponding AUC scores for the four combinations of method-dataset are shown in Figure 4 and the first three rows of Table I, respectively. The RibCage's AUC results outperform the other architectures for all method-dataset combinations, indicating that, on average, for a fixed prediction tolerance, a better Hit Rate is obtained. It is interesting to note that the Siamese architecture is consistently inferior, even with respect to the naive architecture, possibly since the low level features are of high significance.

F. Binary vs Trinary Segmentation Comparison

While conventional segmentation methods provide binary (foreground-background) outputs, the QANet receives trinary (foreground-background-boundary) segmentations. To test which of the representations, the binary or trinary, provide better QA results, we also trained the QANet with binary input representation. The last two rows of Table I present the AUC results for the four method-dataset combinations presented in Section IV-D. The corresponding Hit Rate curves are shown in Figure 5. The comparison shows that trinary segmentation is preferable. This implies that the match (or mismatch) between the boundary class and the actual instance boundaries facilitate the evaluation of the image-segmentation correspondence.

G. Cell Segmentation Benchmark Leader-board Prediction

The prediction capabilities of the QANet were tested on the outputs of BGU-IL(3), CVUT-CZ and KTH-SE(1). Each

Architecture	Segmentation Representation	KTH-SE(1)		CVUT-CZ	
		N2DH-GOWT1	N2DL-HeLa	N2DH-GOWT1	N2DL-HeLa
Naive Network	Trinary	0.890	0.934	0.849	0.914
Siamese Network	Trinary	0.819	0.745	0.804	0.727
RibCage Network	Trinary	0.904	0.947	0.912	0.944
RibCage Network	Binary	0.902	0.933	0.908	0.917

Table I

THE AUC SCORES FOR EVALUATING THE SEGMENTATION PREDICTIONS OF KTH-SE(1) AND CVUT-CZ METHODS ON N2DH-GOWT1 AND N2DL-HeLa DATASETS. THE TABLE COMPARES THREE NETWORK ARCHITECTURE ALTERNATIVES: RIBCAGE NETWORK (WITH BINARY OR TRINARY SEGMENTATION INPUT), SIAMESE NETWORK AND NAIVE NETWORK. THE RIBCAGE NETWORK WITH TRINARY SEGMENTATION INPUTS IS CONSISTENTLY BETTER THAN THE TWO ALTERNATIVES

Evaluated Method	SEG Score	QANet Score	Cross-method Score & Surrogate GT	
BGU-IL(3)	0.811	0.808 (-0.37%)	0.767 (-5.42%)	KTH-SE(1)
CVUT-CZ	0.807	0.813 (+0.74%)	0.769 (-4.70%)	KTH-SE(1)
KTH-SE(1)	0.791	0.799 (+1.01%)	0.772 (-2.40%)	CVUT-CZ

Table II

PREDICTED SEG SCORE RESULTS FOR THE CELL SEGMENTATION BENCHMARK SIM+ DATASET FOR THREE LEADING SEGMENTATION METHODS: BGU-IL(3), CVUT-CZ AND KTH-SE(1) OF THE BENCHMARK. PREDICTION WAS DONE FOR THE **TEST DATA**, WHERE THE GT SEGMENTATIONS OF THIS DATA ARE UNKNOWN TO US. THE TRUE SEG SCORES ARE ACCORDING TO THE BENCHMARK WEB-PAGE. THE TABLE PRESENTS ESTIMATED QANET AND THE CROSS-METHOD EVALUATION WITH RESPECT TO A SURROGATE GT. IN BRACKETS ARE THE RELATIVE ERRORS FROM THE TRUE SEG SCORE

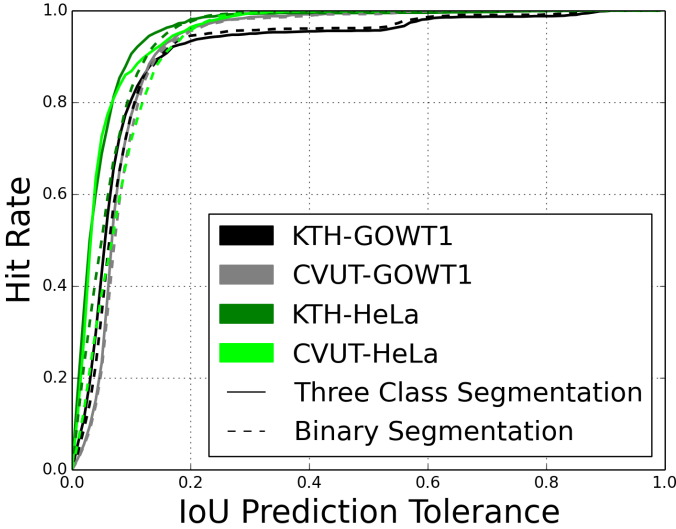


Figure 5. The Hit Rate curves as a function of IoU prediction tolerance for the RibCage Network with either binary (dashed line) or trinary (full line) segmentation input. All configurations were tested using two segmentation methods: KTH-SE(1) (black and dark green) and CVUT-CZ (gray and light green), on two datasets: Fluo-N2DH-GOWT1 (black and gray) and Fluo-N2DL-HeLa (dark and light green)

method was applied to the Fluo-N2DH-SIM+ **test set**. We note that the GT annotations for the test set are unavailable, however the final scores, as validated by the benchmark organizers, are published on the benchmark website. We then measured the mean output of the QANet and the cross method evaluation score. Table II shows the true and predicted SEG scores.

H. Cross-method evaluation and Surrogate Ground Truth

An alternative approach to the QANet could be the cross evaluation between multiple segmentation methods. For example, given two segmentation methods, one could act as a surrogate GT segmentation for the other, and vice versa.

While this approach is valid, we show in the last column of Table II that it is significantly less accurate than the QANet. Our assumption is that regardless of the method - a classical or a machine learning one - segmentation processes are guided by similar principles, therefore, it is not unlikely that different segmentation methods will fail on similar examples and thus fail to evaluate each other.

V. DISCUSSION AND FUTURE WORK

In this paper, we introduced the Quality Assurance Deep Neural Network - QANet - a method for estimating the quality of instance segmentation at the single image level without the need for a human in the loop.

The QANet does not in itself produce a segmentation of an image, but rather predicts a quality measure of a proposed segmentation as if the GT annotation were given. Paraphrasing the British statesman Benjamin Disraeli "...it is easier to be critical than to be correct".

The QANet solves a regression problem getting as input an image with its corresponding proposed segmentation and outputting a scalar representing the estimated quality measure. This is accomplished by a RibCage architecture [2] which inherently compares multi-level, multi-scale features of the two inputs.

During the training phase we cover the entire range of the target quality measure by using synthesized proposed segmentations generated by sampling random deformations of the GT segmentation. Alternatively, if the scores of the proposed segmentations were somehow available, the actual GT segmentations are not required.

The results, based on the publicly available Cell Segmentation Benchmark datasets, presented in Section IV show the QANet's ability to generalize to different datasets and segmentation methods, while being trained only on simulated data. Specifically, the QANet predicted the average IoU score as calculated by the benchmark organizers with maximum relative error of 1%. These result outperform the possible alternative of the surrogate GT as shown in Table II.

The main contribution of the QANet is providing an objective way to assess segmentations of any source. It has practical implications for the endpoint users of the segmentation methods. Moreover, the QANet can be used to alleviate training of segmentation methods either as a ranking function for an active learning frameworks or as a direct loss function for unsupervised training.

REFERENCES

- [1] Arbellet, A., Raviv, T.R.: Microscopy cell segmentation via convolutional lstm networks pp. 1008–1012 (2019)
- [2] Arbellet, A., Riklin Raviv, T.: Microscopy cell segmentation via adversarial neural networks. IEEE ISBI pp. 645–648 (2018)
- [3] Bártošová, E., Šustáček, G., Stixová, L., Kozubek, S., Legartová, S., Foltánková, V.: Recruitment of oct4 protein to uv-damaged chromatin in embryonic stem cells. PLoS One **6**(12), e27281 (2011)
- [4] Dice, L.R.: Measures of the amount of ecologic association between species. Ecology **26**(3), 297–302 (1945)
- [5] Dubuisson, M.P., Jain, A.K.: A modified hausdorff distance for object matching. In: Pattern Recognition, 1994. Vol. 1-Conference A: Computer Vision & Image Processing., Proceedings of the 12th IAPR International Conference on. vol. 1, pp. 566–568. IEEE (1994)
- [6] Goodfellow, I., Pouget-Abadie, J., Mirza, M., Xu, B., Warde-Farley, D., Ozair, S., Courville, A., Bengio, Y.: Generative adversarial nets. In: NIPS. pp. 2672–2680 (2014)
- [7] Jaccard, P.: Étude comparative de la distribution florale dans une portion des alpes et des jura. Bull Soc Vaudoise Sci Nat **37**, 547–579 (1901)
- [8] Magnusson, K.E.G.: Segmentation and tracking of cells and particles in time-lapse microscopy. Ph.D. thesis, KTH Royal Institute of Technology (2016)
- [9] Maška, M., Ulman, V., Svoboda, D., et al.: A benchmark for comparison of cell tracking algorithms. Bioinformatics **30**(11), 1609–1617 (2014)
- [10] Neumann, B., Walter, T., Hériché, J.K., Bulkescher, J., Erfle, H., Conrad, C., Rogers, P., Poser, I., Held, M., Liebel, U., et al.: Phenotypic profiling of the human genome by time-lapse microscopy reveals cell division genes. Nature **464**(7289), 721 (2010)
- [11] Redmon, J., Divvala, S., Girshick, R., Farhadi, A.: You only look once: Unified, real-time object detection. In: CVPR. pp. 779–788 (2016)
- [12] Redmon, J., Farhadi, A.: Yolo9000: better, faster, stronger. In: CVPR. pp. 7263–7271 (2017)
- [13] Redmon, J., Farhadi, A.: Yolo3: An incremental improvement. arXiv preprint arXiv:1804.02767 (2018)
- [14] Ronneberger, O., Fischer, P., Brox, T.: U-net: Convolutional networks for biomedical image segmentation. arXiv preprint arXiv:1505.04597 (2015)
- [15] Sixta, T.: Probabilistic Models for Joint Segmentation, Detection and Tracking. Ph.D. thesis, Czech Technical University in Prague (2019)
- [16] Ulman, V., Maška, M., Magnusson, K., et al.: An objective comparison of cell-tracking algorithms. Nature methods **14**(12), 1141 (2017)
- [17] Wiesner, D., Svoboda, D., Maška, M., Kozubek, M.: Cytovacq: a web-interface for simulating multi-dimensional cell imaging. Bioinformatics (2019)